Inhibition Delay Increases Neural Network Capacity through Stirling Transform

Alain Nogaret*
Department of Physics, University of Bath, Bath BA2 7AY, UK and
Institute for Mathematical Innovation, University of Bath, Bath BA2 7AY, UK

Alastair King
Department of Mathematical Sciences, University of Bath, Bath BA2 7AY, UK

Inhibitory neural networks are found to encode high volumes of information through delayed inhibition. We show that inhibition delay increases storage capacity through a Stirling transform of the minimum capacity which stabilizes locally coherent oscillations. We obtain both the exact and asymptotic formulae for the total number of dynamic attractors. Our results predict a $(\ln 2)^{-N}$-fold increase in capacity for a N-neuron network and demonstrate high density associative memories which host a maximum number of oscillations in analog neural devices.

Inhibitory neural networks bind the electrical activity of different brain regions during tasks such as cognition [1] and memory consolidation [2]. A growing body of evidence suggests that inhibitory interneurons play the central role in entraining cortical circuits [3–5] and emphasizes the importance of synaptic kinetics in triggering synchronized oscillations [5–7]. Dynamical theories [8, 9] have described inhibitory networks as chaotic systems which host a manifold of fixed point attractors activated by external stimulation [10–13]. An understanding of the dependence of the number of attractors on the kinetics of interconnections is now needed to determine the maximum network capacity and to predict the formation of locally coherent oscillations [14] associated with pathological cortical oscillations.

The present paper focuses on the effect of inhibition delay on the oscillatory states of mutually inhibitory neural networks and qualitatively describes the effects of synaptic conductances on the sizes of attractor basins which in turn determine robustness to noise. We show that inhibition delay increases the number of dynamic attractors through a Stirling transform operation [15]. Using *in-silico* neuromorphic models [16], we show that inhibition delay boosts network capacity $(\ln 2)^{-N}$-fold by stabilizing partially coherent oscillations. We obtain the exact analytic and asymptotic expressions of the upper bound of the network capacity, in excellent agreement with the capacity observed at inhibition delays exceeding 1/3 of the duration of an action potential. Analog network implementations demonstrate novel high density associative memories which are robust against noise, temperature and fluctuations in device parameters.

We studied inhibitory networks *in-silico* by interconnecting Hodgkin-Huxley neurons [17] with mutually inhibitory synapses [18]. This approach presents the advantage of integrating multivariate time dependent stimuli without compromising on model accuracy. In particular the use of VLSI synapses allowed the effects of inhibition delay and neurotransmitter kinetics to be fully incorporated in the model. We probed inhibitory networks of various sizes ranging from $N = 3$ to 6 neurons and observed the same general dependence on inhibition delay as in the 4-neuron network (Fig.1). We generated the phase lag maps of the network by stimulating individual neurons, $i = 1 - 4$, with current steps of 25μA amplitude (Fig.1(a)) and by varying their timings in the range $0 \leq \tau_i \leq T$ to change the initial phases of membrane voltage oscillations. T is the period of synchronized oscillations. The phases of neuron oscillations defined the dynamic state of the network. We constructed the phase lag maps by plotting the dephasings of peak voltages from one period to the next and throughout the regime of transient oscillations until the dynamic state reached a fixed point attractor.

A neuron also received postsynaptic inhibitory currents from all other neurons (Fig.1(b)). Dendrite projecting neurons may postpone the onset of inhibition by introducing transmission line delays d which retard the arrival of inhibitory signals at the soma of the postsynaptic neuron. For example, somatostatin interneurons are known to introduce inhibition delays $d = 0 - 800\mu$s by projecting their synapses on the 15μm long dendrites of postsynaptic neurons [19]. When inhibition delay is small $d < 150\mu$s, state trajectories are observed to converge towards six equivalent attractors corresponding to neurons that discharge in the sequence $1 \to 2 \to 3 \to 4$ and its five permutations (Fig.1(c)). Increasing inhibition delay to $d = 400\mu$s stabilizes partially coherent oscillations in which two or more neurons discharge in phase (Fig.1(d)).

Partially coherent oscillations reduce the number of interspike intervals per cycle from N to M with $1 \leq M \leq N$ (Fig.2). These interspike intervals (ISIs) split the N neuron discharges into M distinguishable events of cardinality $k_1 \geq \cdots \geq k_M > 0$ where $k_1 + \cdots + k_M = N$. For example, the 4-neuron network of Fig.1(d) has a single coherent attractor corresponding to all neurons discharging in phase which gives $(k_1, k_2, k_3, k_4) = (4, 0, 0, 0)$ (triangle symbol). Neurons that discharge over $M = 2$ ISIs may distribute as $(3, 1, 0, 0)$ or $(2, 2, 0, 0)$ giving $4+3$ partially coherent attractors (diamond symbols). Over $M = 3$ ISIs, event cardinalities are $(2, 1, 1, 0)$ giving 12

* A.R.Nogaret@bath.ac.uk

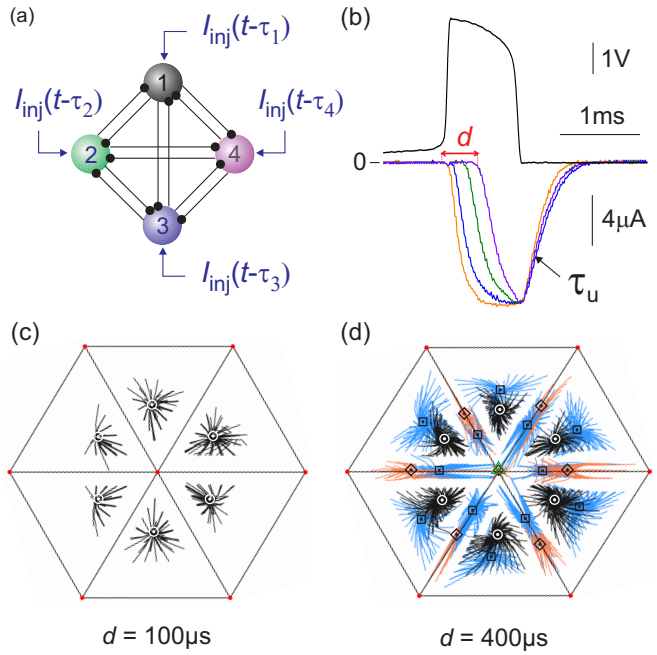

FIG. 1. *(color online)* (a) 4-neuron network with all-to-all reciprocal inhibition. Current steps of amplitude 25μA are injected into neurons 1-4 at times $0 \leq \tau_i \leq T$ $(i = 1-4)$. The timings of current stimuli set the initial conditions of phase lag trajectories. (b) Action potential of the pre-synaptic neuron (black line) and the post-synaptic inhibitory current induced at different inhibition delays $d = 0-500\mu$s (color lines). The kinetics of the post-synaptic current is controlled by the neurotransmitter undocking time τ_u. (c) Orthographic phase portrait of the 4-neuron network measured at small inhibition delay $d = 100\mu$s. The 6 attractors (white circles) correspond to sequential discharge patterns of the 4 neurons. (d) Phase portrait at large inhibition delay $d = 400\mu$s. The additional attractors are partially coherent oscillations with $M = 3$ ISIs per cycle (square symbols), $M = 2$ (diamond symbols) and $M = 1$ for the fully synchronized attractor (triangle symbol).

M	ISI	k_1	k_2	k_3	k_4	n_1	n_2	n_3	n_4	w_N^M	A_N^M	$w_N^M \times A_N^M$
4	$T/4$	**1**	**1**	**1**	**1**	**4**	0	0	0	**1/4**	**24**	**6**
3	$T/3$	**2**	**1**	**1**		**2**	**1**	0	0	**1**	**12**	**12**
2	$T/2$	**3**	**1**			**1**	0	**1**	0	**1**	**4**	**4**
		2	**2**			0	**2**	0	0	**1/2**	**6**	**3**
1	$T/1$	**4**				0	0	0	**1**	**1**	**1**	**1**
												26

TABLE I. Calculation of T_4. $w_N^M = W_N^M/M$.

partially coherent attractors (square symbols). Lastly for $M = 4$, there are 6 sequential attractors $(1, 1, 1, 1)$ (circle symbols). The 4-neuron network therefore hosts 26 attractors in total. The results in Figs.1(c,d) demonstrate that inhibition delay boosts the capacity of the 4-neuron network from 6 to 26 attractors. We now calculate the dependence of network capacity on inhibition delay for a network of arbitrary size.

The list of event occupancies $\{k_i\}$, $i = 1, \ldots, M$ has a dual list $\{n_j\}$, $j = 1, \ldots, N$ which contains the frequency of events of same cardinality. A cycle thus comprises n_1 single spike events, n_2 2-spike events, ... , n_N N-spike events (Table.I) which satisfy the dual sum rule $n_1 + \cdots + n_N = M$. We calculate the total number of attractors by multiplying the number of possible waveforms $W_N^M(n_1, \ldots, n_N)$ obtained by re-ordering events of different cardinalities within a period, with the number of ways of distributing labelled spikes within each waveform $A_N^M(k_1, \ldots, k_M)$ (Fig.2). W_N^M is the number of ways of distributing the M events over N distinguishable slots $n_1, \ldots, n_N$. A_N^M is the number of ways of distributing the N spikes over M distinguishable events of cardinality $k_1, \ldots, k_M$. One obtains:

$$A_N^M(k_1, \ldots, k_M) = \frac{N!}{k_1! \ldots k_M!}, \tag{1}$$

$$W_N^M(n_1, \ldots, n_N) = \frac{M!}{n_1! \ldots n_N!}. \tag{2}$$

Since the product $A_N^M \times W_N^M$ contains M cyclically equivalent trajectories, the total number of attractors is obtained by dividing this product by M and summing over the partition of N $(k \vdash N)$:

$$T_N = \sum_{k \vdash N} \frac{1}{M} \binom{M}{n_1, \ldots n_N} \binom{N}{k_1, \ldots, k_M}. \tag{3}$$

The round brackets are the multinomial coefficients (Eqs.1 and 2). The W_N^M multinomial takes care of the degeneracy arising from permutations within $\{k_i\}$ satisfying $k_1 + \cdots + k_M = N$. This is why the summation is done over $k_1 \geq \cdots \geq k_M > 0$ where M is the number of positive integers in the partition. The capacity of the 4-neuron network is calculated in Table.I. Eq.3 shows that the maximum capacity increases as $T_3 = 6$, $T_4 = 26$, $T_5 = 150$, $T_6 = 1082$, ... $T_N \sim (N-1)!/(\ln 2)^N$, as we shall see below. If one restricts the summation over the partition of N to sequentially discharging neurons, $k_1 = \cdots = k_N = 1$, Eq.3 yields the minimum network capacity: $L_3 = 2$, $L_4 = 6$, $L_5 = 24$, $L_6 = 120$, ... $L_N = (N-1)!$. This increase in capacity occurs as inhibition delay stabilizes partially coherent oscillations, for example from Fig.1(c) to Fig.1(d).

There is actually a direct operation that converts the minimum capacity L_N to the maximum capacity T_N, given by the Stirling transform:

$$T_N = \sum_{M=1}^{N} \left\{ {N \atop M} \right\} L_M \quad N \geq 3\,, \tag{4}$$

where $\left\{ {N \atop M} \right\}$ is the Stirling number of the second kind which counts the number of ways of partitioning the N spikes into M non-empty sets. An explicit formula for the Stirling numbers is:

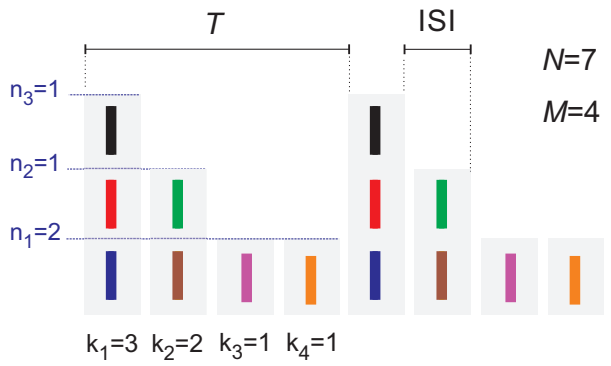

FIG. 2. *(color online)* Distribution of the action potentials (vertical bars) of a 7-neuron network over 4 events separated by interspike intervals (ISI) of duration $T/4$. Action potentials repeat with the periodicity of synchronized oscillations T. The number of spikes occupying each time slot - or event - is $(k_1, k_2, k_3, k_4) = (3, 2, 1, 1)$. The frequencies of events of same cardinality are $(n_1, n_2, n_3, n_4, n_5, n_6, n_7) = (2, 1, 1, 0, 0, 0, 0)$.

$$\left\{ \begin{matrix} N \\ M \end{matrix} \right\} = \frac{1}{M!} \sum_{j=0}^{M} (-1)^{M-j} \left(\begin{matrix} M \\ j \end{matrix} \right) j^N. \qquad (5)$$

In order to derive the asymptotic form of T_N, it is useful to introduce the sequence of Fubini numbers, $R_N = \sum_{k \vdash N} W_N^M A_N^M$, which differs from T_N by counting the linearly ordered trajectories of an N-neuron network. The two sequences are related by $T_N = 2R_{N-1}$ $(N \geq 3)$ since omitting a reference neuron gives a 2:1 correspondence between the *cyclically* ordered trajectories of the N-neuron network and the *linearly* ordered trajectories of the $N-1$-neuron network excluding the reference neuron.

One seeks the exponential generating function $R(z)$ of R_N. As observed by Good [20], the term $1/(k_1! \ldots k_M!)$ which appears in A_N^M is the coefficient of $z^{k_1+\cdots+k_M}$ in the expansion of:

$$\left(\sum_{k_1=1}^{\infty} \frac{z^{k_1}}{k_1!} \right) \cdots \left(\sum_{k_M=1}^{\infty} \frac{z^{k_M}}{k_M!} \right) = (e^z - 1)^M. \qquad (6)$$

Using $k_1 + \cdots + k_M = N$ and summing over events M, one obtains the generating function $R(z)$ as:

$$\sum_{M=0}^{\infty} (e^z - 1)^M = \sum_{N=0}^{\infty} \sum_{k \vdash N} W_N^M \frac{N!}{k_1! \ldots k_M!} \frac{z^N}{N!}, \qquad (7)$$

which simplifies by replacing the left hand side with its geometric series and the coefficient of $z^N/N!$ with R_N:

$$\frac{1}{2 - e^z} = \sum_{N=0}^{\infty} R_N \frac{z^N}{N!}. \qquad (8)$$

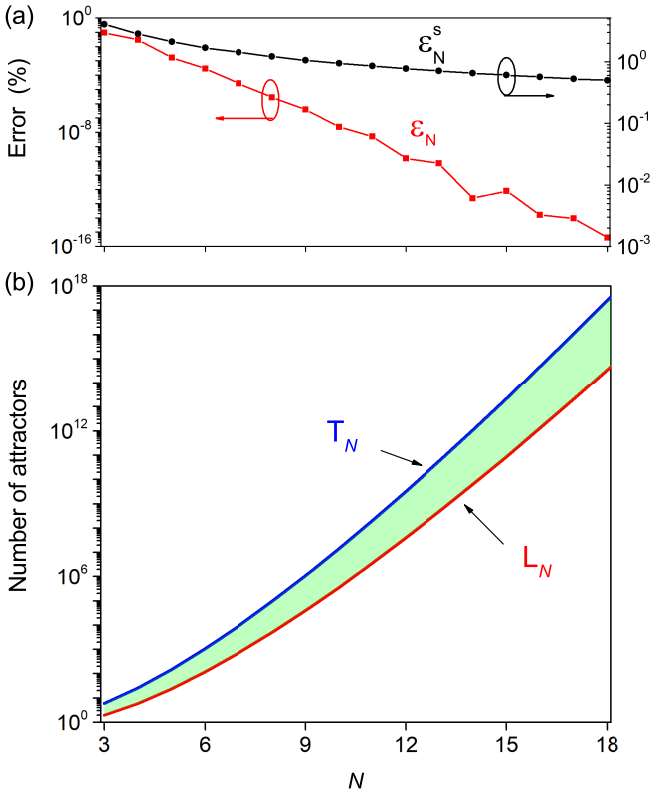

FIG. 3. *(color online)* (a) Asymptotic errors ϵ_N and ϵ_N^s plotted as a function of network size. (b) Upper and lower boundaries of the network capacity: T_N and L_N. The capacity of experimental networks is T_N for inhibition delays larger than 1/3 of the duration of an action potential. For smaller delays, the network capacity lies in the shaded region between L_N and T_N.

$R(z)$ has a pole at $z = \ln 2$ where the series diverges. Near this pole, the terms $z^N/N!$ at large N dominate in the series which allows the asymptotic value of R_N to be calculated [21]. Expanding $R(z)$ about the pole, one obtains:

$$\frac{1}{2 - e^z} = \sum_{N=0}^{\infty} \frac{N!}{2(\ln 2)^{N+1}} \left(1 + \frac{(\ln 2 - z)^2}{2z} + \ldots \right)^N \frac{z^N}{N!}. \qquad (9)$$

Identifying the coefficients of $z^N/N!$ in Eqs.9 and 8 at $z \to \ln 2$ yields the asymptotic formula of R_N. Recalling that $T_N = 2R_{N-1}$ the asymptotic value of the maximum capacity follows as:

$$T_N \sim \frac{(N-1)!}{(\ln 2)^N}, \qquad N \geq 3 \qquad (10)$$

$$\sim \frac{\sqrt{2\pi(N-1)}}{\ln 2} \left(\frac{N-1}{e \ln 2} \right)^{N-1}. \qquad (11)$$

Eq.10 is a highly accurate estimate of the total number of attractors. The relative error is $\epsilon_3 = 9 \times 10^{-4}$ $(N = 3)$,

$\epsilon_{20} = 7 \times 10^{-20}$ ($N = 20$) and decreases as $\epsilon_N \sim 10^{-N}$ (Fig.3(a), square symbols). The capacity of larger networks may be estimated using Stirling's approximation of the factorial (Eq.11). In this case the relative error decreases as $\epsilon_N^s \sim 1/N$ (Fig.3(a), dot symbols).

When inhibition delay is small ($d < 150\mu$s), network capacity scales with network size according to sequence L_N (Fig.3(b)). Large inhibition delays ($d > 300\mu$s) increase capacity $(\ln 2)^{-N}$-fold to T_N by stabilizing partially coherent oscillations (Fig.3(b)). At intermediate delay ($150\mu\text{s} \leq d \leq 300\mu$s), the network only supports oscillations with low coherence ($M \to N$) which are the most robust. As a result, the network capacity lies between L_N and T_N (Fig.3(b), shaded region). Biological neurons may establish up to 10^4 connections with other neurons. In the absence of noise, an all-to-all network the size of the neuron connectome would boost its capacity $10^{1,592}$-fold to $10^{37,250}$ attractors by increasing inhibition delay up to 1/3 of the duration of the action potential.

Eq.11 introduces constant $\eta = e \ln 2$ whose physical meaning we elucidate by calculating the rate of change of capacity with network size. We find $dT_N/dN \sim [1 + \ln((N-1)/\eta)]T_N$. We then seek the size of the network N_g whose capacity increases g-fold upon the addition of an extra neuron ($\Delta N = 1$). Since $\Delta T_N/T_N = g - 1$, one obtains $N_g \sim 1 + \eta e^{g-2}$. It follows that one extra neuron will double the capacity of a 3-neuron network, decuple the capacity of a 5617-neuron network, and increase 20-fold the capacity of a hypothetical network 1% the size of the human cerebral cortex (120 million neurons). $\eta = (N_g - 1)/e^{g-2}$ thus defines the growth rate of the network with capacity gain. The larger the network, the greater the effect a tiny size increment will have in boosting capacity, both in absolute and relative terms. Using these principles, our inhibitory networks (Fig.1(d)) demonstrate associative memories which have greater memory capacity than winnerless networks $\sim (N-1)!$ [9] and Hopfield networks $\sim 0.14N$ [22].

Experiments in Fig.1 show that the maximum capacity is robust in a noisy environment consisting of synaptic current noise (Fig.1(b)), contact noise, current stimulus noise, component-to-component deviations, and fluctuations in synaptic conductances. This further demonstrates the known robustness of dynamical encoding of stimuli by heteroclinic activation paths [9]. Changing synaptic conductances has the effect of varying the sizes of basins of attraction relative to one another [11]. The residual imbalance of synaptic conductances in the experimental network breaks the 6-fold symmetry of phase portraits in Figs.1(c,d). Basins of attraction protect dynamical attractors from decoherence by noise. This is why the maximum network capacity can always be observed at a finite noise level provided inhibition delay is sufficient. At large values of N, the number of dynamical attractors increases faster than the volume of phase space. This makes the average attractor radius decrease as $\eta/(N-1)$. Memories implemented in physical hardware will thus have finite immunity to noise at any N but their tolerance to noise will tend to zero when $N \to \infty$. These conclusions may be extended to bursting neuron networks [23, 24].

ACKNOWLEDGMENTS

We thank Ashok Chauhan and Joseph Taylor for discussions. This work was supported by the European Union's Horizon 2020 Future Emerging Technologies Programme (Grant No. 732170) and the British Heart Foundation under grant NH/14/1/30761.

[1] J. Yamamoto, J. Suh, D. Takeuchi, and S. Tonegawa, Cell **157**, 845 (2014).
[2] R. Boyce, S. D. Glasgow, S. Williams, and A. Adamantis, Science **352**, 812 (2016).
[3] M. Bartos, I. Vida, and P. Jonas, Nature Review Neuroscience **8**, 45 (2007).
[4] M. M. Huntsman, D. M. Porcello, G. E. Homanics, T. M. DeLoery, and J. R. Huguenard, Science **283**, 541 (1999).
[5] J. Veit, R. Hakim, M. P. Jadi, T. J. Sejnowski, and H. Adesnik, Nature Neuroscience **20**, 951 (2017).
[6] V. S. Sohal, F. Zhang, O. Yizhar, and K. Deisseroth, Nature **459**, 698 (2009).
[7] J. A. Cardin, M. Carlen, K. Meletis, U. Knoblich, F. Zhang, K. Deisseroth, L.-H. Tsai, and C. I. Moore, Nature **459**, 663 (2009).
[8] S. Atasoy, I. Donnelly, and J. Pearson, Nature Communications **7** (2016).
[9] M. Rabinovich, A. Volkovski, R. Lecanda, R. Huerta, H. D. I. Abarbanel, and G. Laurent, Physical Review Letters **87**, 068102 (2001).
[10] A. Shilnikov, R. L. Calabrese, and G. Cymbalyuk, Physical Review E **71**, 056214 (2005).
[11] J. Wojcik, J. Schwabedal, R. Clewley, and A. L. Shilnikov, PLoS ONE **9**, e92918 (2014).
[12] C. C. Canavier, D. A. Baxter, J. W. Clark, and J. H. Byrne, Biological Cybernetics **80**, 87 (1999).
[13] Y. Manor and F. Nadim, The Journal of Neuroscience **21**, 9460 (2001).
[14] M. Le Van Quyen, L. E. Muller II, B. Telenczuk, E. Halgren, S. Cash, N. G. Hatsopoulos, N. Dehghani, and A. Destexhe, PNAS **113**, 9363 (2016).
[15] M. Bernstein and N. J. A. Sloane, Linear Algebra and its applications **226-228**, 57 (1995).
[16] L. Zhao and A. Nogaret, Physical Review E **92**, 052910 (2015).
[17] M. Mahowald and R. Douglas, Nature **354**, 515 (1991).
[18] C. Bartolozzi and G. Indiveri, Neural computation **19**, 2581 (2007).
[19] J. C. Fiala and K. M. Harris, "Dendrites," (Oxford University Press, Great Clarendon Street, Oxford, OX2 6DP,

1999) Chap. 1, pp. 1–34.
[20] I. J. Good, Fibonacci Quaterly **13**, 11 (1975).
[21] P. Flajolet and R. Sedgewick, *Analytic Combinatorics* (Cambridge University Press, 2009).
[22] D. J. Amit, H. Gutfreund, and H. Sompolinsky, Physical Review Letters **55**, 1530 (1985).
[23] E. Marder, D. Bucher, D. J. Schulz, and A. L. Taylor, Current Biol. **15**, R685 (2005).
[24] A. Nogaret, L. Zhao, D. J. A. Moraes, and J. F. R. Paton, Journal of Neuroscience Methods **212**, 124 (2013).